Visual Neuroscience (2008), **25**, 289–299. Printed in the USA.

doi:10.1017/S0952523808080371

Number and topography of cones, rods and optic nerve axons in New and Old World primates

BARBARA L. FINLAY,[1] EDNA CRISTINA S. FRANCO,[2] ELIZABETH S. YAMADA,[2] JUSTIN C. CROWLEY,[1]* MICHAEL PARSONS,[1] JOSÉ AUGUSTO P.C. MUNIZ,[3] AND LUIZ CARLOS L. SILVEIRA[4]

[1]Departments of Psychology and Neurobiology and Behavior, Cornell University, Ithaca, New York
[2]Universidade Federal do Pará, Centro de Ciências Biológicas, Departamento de Fisiologia, Belém, Pará, Brasil
[3]Centro Nacional de Primatas, Ananindeua, Pará, Brasil
[4]Universidade Federal do Pará, Núcleo de Medicina Tropical, Belém, Pará, Brasil

(RECEIVED October 5, 2007; ACCEPTED February 11, 2008)

Abstract

To better understand the evolution of spatial and color vision, the number and spatial distributions of cones, rods, and optic nerve axon numbers were assessed in seven New World primates (*Cebus apella*, *Saimiri ustius*, *Saguinus midas niger*, *Alouatta caraya*, *Aotus azarae, Calllithrix jacchus*, and *Callicebus moloch*). The spatial distribution and number of rods and cones was determined from counts of retinal whole mounts. Optic axon number was determined from optic nerve sections by electron microscopy. These data were amassed with existing data on retinal cell number and distribution in Old World primates, and the scaling of relative densities and numbers with respect to retinal area, eye and brain sizes, and foveal specializations were evaluated. Regular scaling of all cell types was observed, with the exceptionally large, rod-enriched retina of the nocturnal owl monkey *Aotus azarae*, and the unusually high cone density of the fovea of the trichromatic howler monkey *Alouatta caraya* presenting interesting variations on this basic plan. Over all species, the lawful scaling of rods, cones, and retinal ganglion cell number is hypothesized to result from a conserved sequence of cell generation that defends retinal acuity and sensitivity over a large range of eye sizes.

Keywords: Retina, New and Old World primate, Cone, Rod, Optic nerve, Retinal ganglion cell, Allometry, Fovea

Introduction

The anthropoid neural retina has the fundamental conformation, and organization of photoreceptors and neurons characteristic of all vertebrates, but features the integrally related specializations of high acuity, trichromacy and ocular motility associated with adaptation to diurnality, in the context of its original nocturnal roots (Ross, 2000; Heesy & Ross, 2001). These features of anthropoid optics, the fovea, great ocular motility, and trichromacy, have been the subject of intense study in humans and the typical experimental animal for this work, the rhesus macaque. To understand the overall parameters of retinal organization from which the anthropoid eye derives, however, a much broader comparative base is necessary. For this, the multiple species of New World primates offer excellent contrasts in retinal organization.

Address correspondence and reprint requests to: Barbara L. Finlay, Department of Psychology, Uris Hall, Cornell University, Ithaca, NY 14853. E-mail: blf2@cornell.edu

*Present address: Department of Biological Sciences, Center for the Neural Basis of Cognition and Lane Center for Computational Biology, Carnegie Mellon University, Pittsburgh, PA 15213.

Old World Anthropoidea (which comprise anthropoid apes, humans, and monkeys), and New World Anthropoidea (the New World monkeys) are thought to have been derived from a common diurnal ancestor, with a founder population of New World monkeys who somehow rafted from Africa to South America 40 million years ago (Fleagle, 1988). New World monkeys (Infraorder *Platyrrhini*) have undergone a wide and successful speciation, invading all levels of forest canopy and multiple dietary niches. All are diurnal, except the owl monkey (*Aotus sp.*), which has re-invaded the nocturnal niche. A wide range of eye and body sizes, at least six variations of mono-, di-, and trichromacy, and variations in foveal organization exist, as well as the nocturnalized retina (Jacobs et al., 1996; Jacobs, 1998; Kainz et al., 1998; Heesy & Ross, 2001). In the present study, we have attempted to look at a wide range of variability (subject, of course, to species availability) while including those New World monkeys that have already been the subject of experimental study to maximize integration with existing data. These monkeys include representatives of the three major Families (Schneider et al., 1996; Nagamachi et al., 1999; Schneider, 2000) one from the *Atelidae*, the howler monkey, *Alouatta caraya*, which is a large folivore and the only known "obligatory" trichromat genus of the platyrrhines; one from

the *Pitheciinae*, the titi monkey *Callicebus moloch*, a small omnivore which has a polymorphic color vision comprising a population of di- and trichromatic individuals with five different alleles for the M/L photo pigments; and four from the family *Cebidae*. From the last family, there are two from the subfamily *Cebinae*, *Cebus apella*, the often-studied large-brained capuchin monkey, and the smaller squirrel monkey, *Saimiri ustius*; and two from the subfamily *Callitrichinae*, the tamarin monkey, *Saguinus midas niger* and the marmoset *Callithrix jacchus*. These four diurnal Cebidae also have polymorphic color vision comprising populations of di- and trichromats with three different alleles for the M/L photo pigments. Finally, from *Aotinae*, we studied the owl monkey *Aotus azarae*. With the exception of *Aotus*, the nocturnal monochromat, all of the latter have foveas for high-acuity diurnal vision, and the variation of trichromacy in which a large fraction of the females are trichromats, and the males dichromats (Jacobs, 1998).

After describing the retinal organization of these species, and comparing them to Old World primates, anthropoid apes, and humans, we will frame the evolution of species-typical eyes and retinas in terms of the minimal alterations of a common developmental program (Gerhart & Kirschner, 1997; Finlay et al., 2005). Preliminary reports of these studies have been made (Snow et al., 1997; Silveira et al., 2001, 2004, Finlay et al., 2007; Franco et al., 2007).

Materials and methods

Animals

All animals were provided by the Centro Nacional de Primatas (CENP, Ananindeua, Pará, Brazil), a breeding and cachement facility for northern Brazil, and were collected over a 10 year period as part of a larger study. We analyzed retinas and optic nerves from three *Cebus apella*, four *Saimiri ustius*, three *Saguinus midas niger*, three *Aotus azarae*, four *Alouatta caraya*, two *Callithrix jacchus jacchus*, and one *Callicebus moloch*. Note that in the initial investigations of *Aotus* (Silveira et al., 1993) the species under study has been reclassed as *Aotus azarae* and not *Aotus trivirgatus*; it is the same animal with a different species name. Details of sex, weight, and tissue sampled for all animals can be found in Table 1. All animal care and procedures were approved by local animal care and use committees, as well as Cornell University IACUC in accord with NIH Guidelines regarding the care and use of animals for experimental procedures; no animals were classified as endangered at the time of collection.

Preparation of retinas, brains, and optic nerves

Animals were lightly anesthetized with intramuscular injection of a mixture 4:1 of 2% xylazine hydrochloride (Rompum, Bayer,

Table 1. *Rod, cone, and optic nerve numbers, individual New World monkeys*

Species	Individ.	Sex	Br wt (g)	Bo wt (kg)	R/L	Ret area (mm^2)	# cones	# rods	# Axons
Cebus	Stuart	M	62.0		L	455	3,798,460	55,060,093	
					R	454	3,853,230	45,121,826	
	880425	M	62.0		R	575	4,486,339	47,458,781	
					L	541	4,295,170	48,856,446	
	951227	M	71.0		R	576	5,258,207	57,015,172	1,076,696
					L	637	5,364,746	61,331,721	
Saimiri	96109A	M	21.6		R	293	3,605,376	35,345,904	875,005
					L				833,936
	960109b	M	25.7		R	365	3,519,988	38,511,202	821,529
	960109C	F	19.8		R	408	2,941,289	28,269,440	879,529
	970119	M	27.8	0.33	L	341	3,486,504	32,326,612	
Callithrix	960518	F	7.9		R	184	3,587,937	9,786,595	
	960304	M	7.9		R	224	3,881,809	11,533,809	
Saguinus	960110B	M	9.1	0.48	R	258	4,097,219	11,055,429	
	97108B	F	9.1	0.44	L				672,500
	960111A	F	9.6	0.40					682,000
Callicebus	960111B	F	16.6	0.91	R				695,000
					L				706,000
Alouatta	971010A	M	59.6	4.80	R	433	2,939,343	58,505,135	
					L				1,190,000
	970111A	M	54.3	4.60	R	483	4,176,895	66,694,904	
	980114	F	40.0	1.85	L				965,000
	980115	F	44.0	2.29	R	415	3,724,828	55,117,631	1,088,000
					L	453	3,447,722	54,628,650	1,081,000
Aotus	970114A	M	14.9	0.52	R				430,000
	980115A		14.9		L				480,000
	980115B	F	15.0	0.59	R	635	2,389,765	158,777,328	
					L	557	2,205,835	122,513,951	578,000

Porto Alegre, Brazil) and 5% ketamine hydrochloride (Ketalar, Parke-Davis, São Paulo, Brazil), and dark adapted for one-half hour. They were deeply anesthetized with the same mixture and perfused by phosphate buffered saline solution (PBS). The cornea and vitreous were removed and the eye was postfixed for 10–15 min in formol saline and dissected rapidly away from the choroid. The retina was postfixed for 2 h in 10% formol saline. The retina was flat-mounted on a nongelatinized slide with photoreceptors layer upper and cleared with dimethylsulfoxide overnight, rinsed, covered with a mixture 3:1 of glycerol and distilled water, and the coverslip sealed with nail polish (Curcio et al., 1987).

Cones and rods were counted along the horizontal, vertical and two oblique meridians using a binocular microscope under 100× oil immersion objective. In the central region, sampled regions were located at 0, 0.05, 0.1, 0.25, 0.5, and 0.75 mm from the center of the fovea. From 1 mm toward the periphery, counts were made every 1 mm. For cone counts, the sampled areas were 256 μm^2 between 0 and 0.1 mm; 1024 μm^2 between 0.25 and 1 mm; and 6400 μm^2 from distances 2 mm of the fovea. For rod counts, a single sampling area of 1024 μm^2 was used for all locations. Isodensity contours were constructed and the number of cones and rods along the retina estimated from integration of the density values.

Following perfusion and eye dissection, brains were removed from their skulls and weighed, including olfactory bulbs, and the medulla to the level of the pyramidal decussation. Because our ultimate interest is to describe retinal development with respect to whole brain development, comparison of retinal cell numbers to brain weight allows us to compare these results to developmental and allometric studies of the brain (Stephan et al., 1981; Finlay et al., 2005).

For electron microscopy, optic nerve sections were removed from just behind the orbit at the time of eye dissection and stored in 2% glutaraldehyde. Samples were fixed in 2% paraformaldehyde/3% gluteraldehyde in a 0.1M sodium cacodylate buffer, pH 7.4 for 1 h, reacted with 2% osmium tetroxide, and embedded in Spurr's resin. Sections were cut on a Reichert OMU2 Ultramicrotome; thick sections were used to measure optic nerve area. Thin sections were placed on formvar coated 2 mm Gilder aperture grids (Ted Pella) and stained with 2% uranyl acetate and lead citrate. The smallest nerves could be visualized completely within the grid; for larger nerves, either two or four contiguous sections were mounted to produce an unobstructed view of the right, left, top, and bottom aspects of the optic nerve as necessary. Images were taken on a Fei Tecnai 12 Biotwin TEM using a Gatan 689 CCD camera with Digital micrograph software at 200 μm intervals in a regular grid oriented randomly with respect to the sample at 11,500× magnification. The percentage of each sample's area of the entire optic nerve face was calculated. Myelinated and unmyelinated axons were counted with appropriate stereological procedures to prevent double counting, and the results integrated to produce the entire optic nerve count. Except where noted (Table 1), only one optic nerve was sampled per animal.

Overall quantification

Table 1 lists the results of individual animals, detailing those instances where both the right and left retina and optic nerve were assessed; for those few instances where brain weights were not available, the average of the other recorded animals of the same species was used for subsequent analyses. Table 2 sums the results to a single value for rod, cone, or optic nerve number for each species for this study, and adds results from other comparable studies, including Old World primates, with their sources indicated. The simple average of multiple studies was taken, when available, to produce the listed total rod, cone, or optic nerve numbers. Simple regressions were the only descriptive statistics used.

Results

Appearance of the photoreceptor mosaic

Cones and rods were readily distinguished in flat mounted retinas cleared with dimethylsulfoxide. The morphology and size of outer and inner segment, especially when observed step-by-step from the periphery toward the foveola allowed these two classes of photoreceptors to be distinguished and counted. This criterion was used to differentiate the two cellular types in all the analyzed eccentricities, but required a minute inspection in the central region from the fovea to 2 mm of eccentricity. Fig. 1 illustrates the cone mosaic at the same retinal eccentricity for different primates.

Table 2. *Cones, rods, and optic nerve axons by species*

Species	Brain wt (g)	ON#	Cone#	Rod #	Ret area (mm^2)
Cebus apella	61.6	1,092,800	4,532,100	52,849,500	565
Saimiri ustius	7.8	851,800	3,438,000	33,613,000	352
Callithrix jacchus	7.8		3,427,400	10,660,000	206
Saguinus midas niger	9.2	677,250	4,097,000	11055429	258
Callicebus moloch	16.6	700,500			
Alouatta caraya	49.48	1,084,500	3,567,504	60,024,393	444
Homo sapiens	1330.0	1,158,000	4,450,000	92,000,000	909
Macaca mulatta	90.0	1,468,400	3,100,000	61,000,000	670
Papio anubis	201.0	1,580,000			793
Cercopithecus aethiops	59.8	1,228,600			707
Aotus azarae	15.4	480,000	2,297,800	140,645,600	595

(Additional sources. *Aotus*: Ogden (1975); Wikler & Rakic (1990); Silveira et al. (1993); *Cebus*: Silveira et al. (1989); Andrade da Costa & Hokoç (2000); *Callithrix*: Troilo et al. (1993); Wilder et al. (1996); *Cercopithicus*: Herbin et al. (1997); *Homo*: Curcio et al. (1990); Jonas et al. (1992); Cull et al. (2003); *Macaca*: Perry & Cowey (1985); Wikler et al. (1990); *Papio*: Fischer & Kirby (1991))

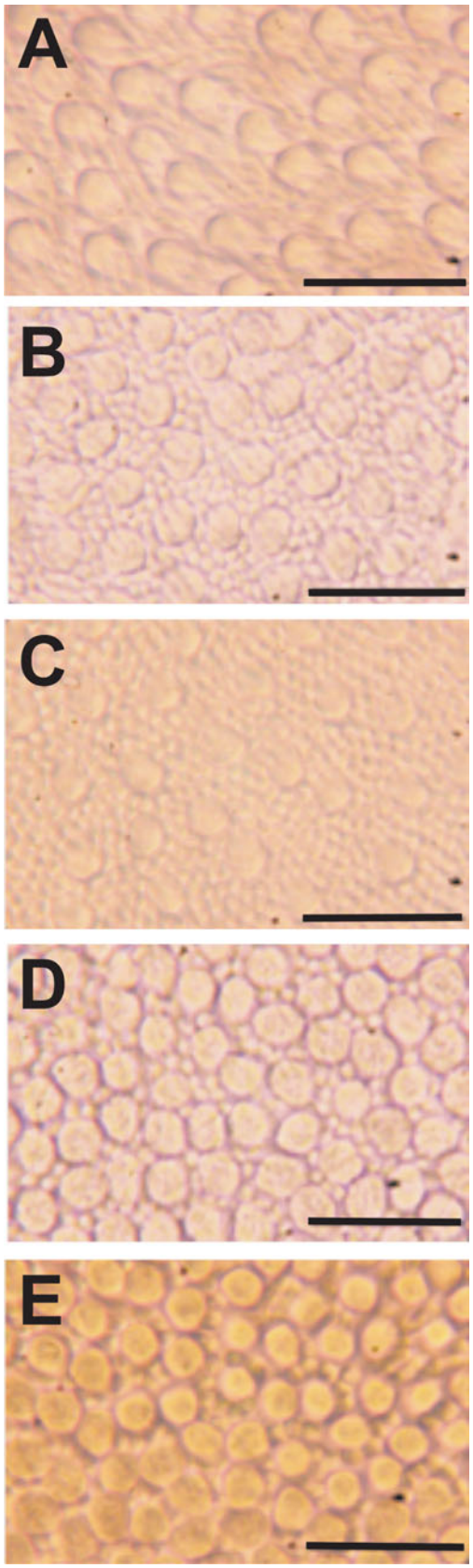

Fig. 1. Photomicrographs of photoreceptor mosaic in the diurnal primates retinas at 5 mm eccentricity nasal. Scale bar = 20 μm. (**A**) *Cebus apella*; (**B**) *Saimiri ustius*; (**C**) *Alouatta caraya*; (**D**) *Saguinus midas niger*; (**E**) *Callithrix jacchus jacchus*.

Cone density in diurnal and nocturnal species

The peak of cone density for five diurnal species was located in the foveola (Figs. 2, 3). The mean values (in cones/mm^2 ± s.d.) were: 394,532 ± 49,719 for *Alouatta* (n = 2), which is more than twice the peak cone density reported in any other New or Old World monkey (Franco et al., 2000). Peak cone density was 164,062 ± 13,811 for *Cebus* (n = 5); 138,021 ± 8,132 for *Saimiri* (n = 3); 150,391 ± 2,762 for *Saguinus* (n = 2); and 132,813 ± 27,622 for *Callithrix* (n = 2). Andrade da Costa and Hokoç (2000) find a similar peak density for *Cebus*, 173,909 ± 74,000, and Troilo et al. (1993) find a rather lower peak density for *Callithrix* of 190,600 ± 15,600 (n = 6) as do Wilder et al. (1996), 211,000 cones/mm^2. Sources of variable peak cone density are discussed at more length in a prior paper (Franco et al., 2000)

The cone density decreased in the first millimeter of foveola. The average of density of cones in the medium and peripheral region of the retina was 8,760 ± 0,843 for *Alouatta*; 8,901 ± 1,284 for *Cebus*; and 9,919 ± 1,182 for *Saimiri*. The density of cones in the equivalent region of retina in the smaller retinas of *Callithrix* and *Saguinus* were much higher. These primates possess high densities of cones with values around 19,802 ± 3,311 for *Saguinus* and 22,778 ± 3,601 for *Callithrix*.

In the retina of the *Aotus*, the peak of cone density was found in the central retina with average values of 17,090 ± 6,215 cones/mm^2 (Fig. 2). These values had diminished to 8,463 ± 2,458, 7,812 ± 1,692, 7,161 ± 1,128, and 6,185 ± 1,492 at 1 mm of eccentricity in the temporal, nasal, ventral, and dorsal regions, respectively. The cone density in the medium and peripheral region of the retina of *Aotus* was of 4,466 ± 0,351 to 3,618 ± 0,562 in the nasal and dorsal region (Figs. 2A and 2C). The values found in the present study are higher than those reported by Ogden (1975) are and Wikler and Rakic (1990).

Rod density in diurnal and nocturnal species

Diurnal primates have a rod-free region in the center of the fovea. For three of our four diurnal primates, rods were first observed approximately 250 μm from the center of the fovea. In *Alouatta*, however, distinct rods could be observed at only 100 μm of eccentricity, the same animal in which the cone density was twice the others'. The *Aotus* retina does not possess a rod-free region. In diurnal species, the greatest density of rods was eccentric to the fovea, approaching the papilla of the optic nerve of each species. The greatest density of rods was observed in the dorsal region in the majority of the species studied. The rod peak density was (in rods/mm^2 ± s.d.) 209,228 ± 51,576 for *Alouatta*; 174,967 ± 42,132 for *Cebus*; 37,939 ± 23,046 for *Saimiri*; 87,646 ± 44,569 for *Saguinus*; and 79,102 ± 13,811 for *Callithrix*. All diurnal species had a naso-temporal asymmetry, with greater values in the nasal region than the temporal region (Figs. 2B and 2D). In *Aotus*, the rods were packed densely and rod density varied from 388,020 ± 103,535 in the central region of the retina to 399,413 ± 11,881 at 2 mm of eccentricity in the temporal region (Table 2). Figs. 3 and 4 show representative maps of isodensity lines for cones and rods for one whole retina of each diurnal species. In the maps for cones, we can see that the contours have a horizontally elongated conformation, a visual streak. The same has been observed in the *Cebus* retina (Andrade da Costa & Hokoç, 2000), *Macaca nemestrina* retina (Packer et al., 1989), and human retina (Curcio et al., 1990).

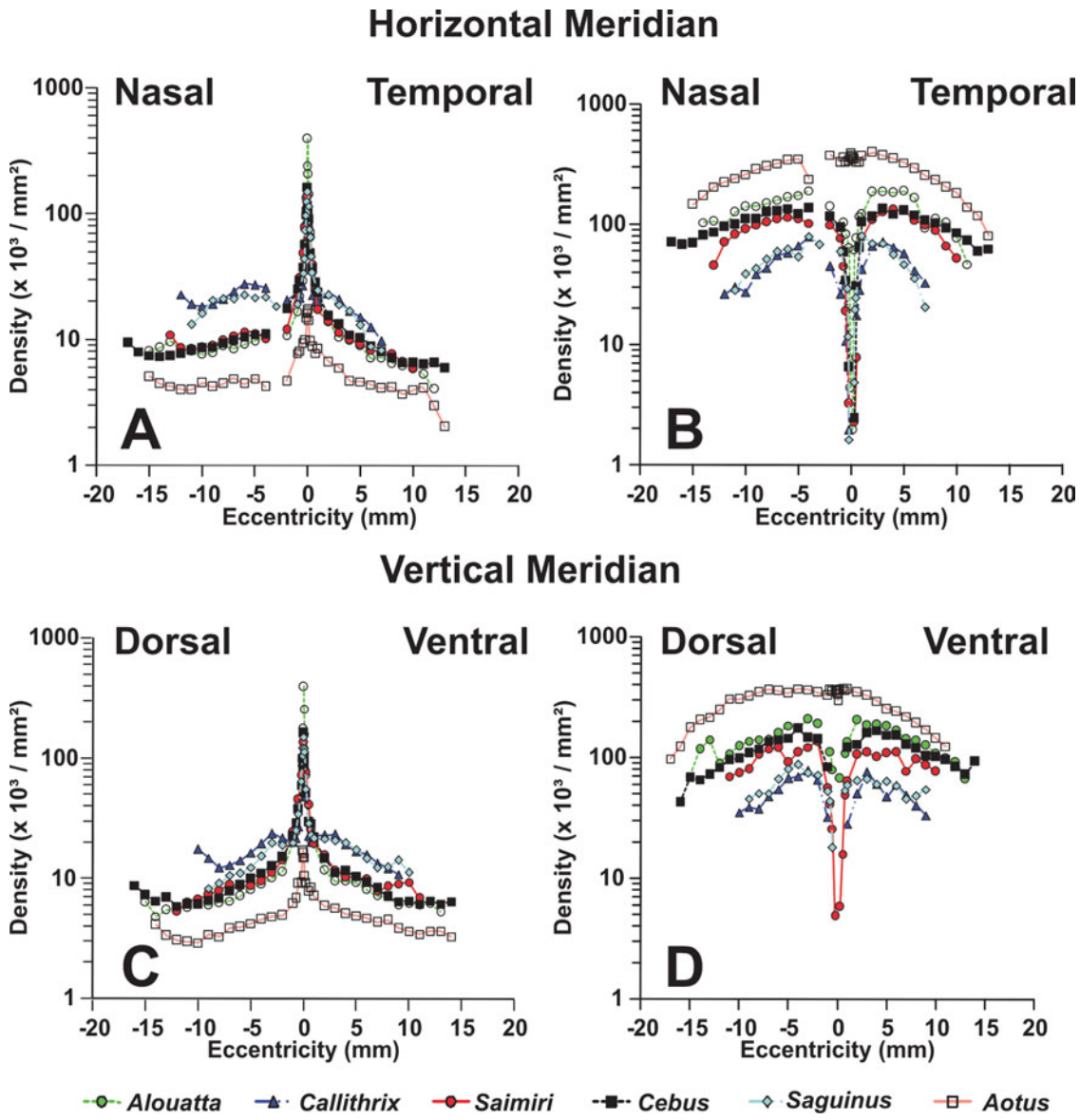

Fig. 2. Photoreceptor density as a function of eccentricity from fovea to the periphery along the horizontal (**A** and **B**) and vertical (**C** and **D**) meridians. Cone density (A and C) and rod density (B and D).

Estimate of the total number of cones and rods

Cone and rod totals were estimated by integrating the density values along the retina (as in Figs. 3 and 4). Individual animal values are listed in Table 1, and graphed, indexed against each species' brain weight, in Figs. 5A and 5B; and species' means, including additional Old World primate data in Fig. 6. We observed somewhat more total cones in *Cebus* than counted by Andrade da Costa and Hokoç (2000), 4.5 versus 3.8 million, though rod numbers were identical, and also more total cones in *Callithrix*, 3.7 versus 2.8 million (Troilo et al., 1993). Note the slight diminution of cones in *Aotus* compared to its large excess of rods. For diurnal primates, there is no apparent relationship of cone number to brain size, while rods track brain size reasonably closely.

Estimate of retinal ganglion cell numbers from optic nerve electron microscopy

Qualitative inspection of the organization of optic axons revealed no notable deviations from the extensive literature on the primate optic nerve (Rakic, 1983; Reese & Ho, 1988; Jonas et al., 1992; Naito, 1996; Cull et al., 2003). Axons were of variable size and the very large majority myelinated, with no striking associations with retinal area, brain or body size, or with nocturnality (*Cebus*, 93.4%; *Saguinus*, 94%; *Alouatta*, 93.5%, *Aotus*, 94.2%). Excluding *Aotus*, optic nerve axon numbers scaled regularly with brain size, but at a markedly flatter slope than rods (Table 1, Fig. 5). *Aotus* optic axon and cone numbers are both slightly lower than the number expected from a diurnal monkey of the same brain size.

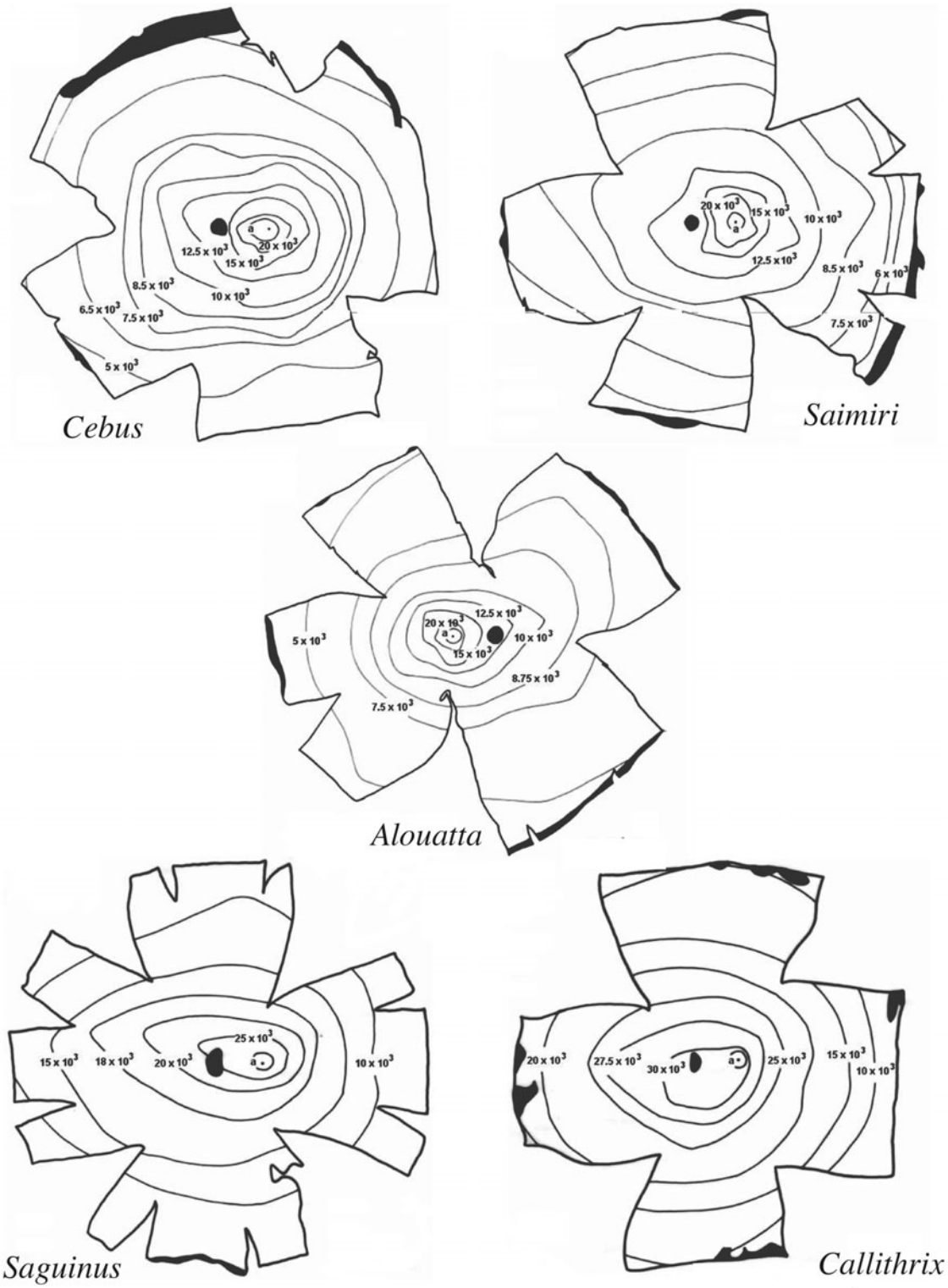

Fig. 3. Map of cone density in (**A**) *Cebus* (area = 454 mm^2) Isodensity line a = 25 × 10^3, (**B**) *Saimiri* (area = 365 mm^2) Isodensity line a = 50 × 10^3, (**C**) *Alouatta* (area = 453 mm^2) Isodensity line a = 40 × 10^3, (**D**) *Saguinus* (area = 245 mm^2) Isodensity line a = 30 × 10^3, and (**E**) *Callithrix* (area = 184 mm^2) Isodensity line a = 50 × 10^3. Variable scale as indicated by areal measurements.

Overall allometric scaling

In Table 2 and Fig. 6, the grand mean for each New World Monkey species is plotted, and values for *Macaca mulatta, Cercopithecus aethiops, Papio anubis*, and *Homo sapien*s are added, from the published literature; unlike Fig. 5, which is a semilog plot to best illustrate individual variability, Fig. 6 is a log-log plot. These additional species have the same pattern seen in the New World

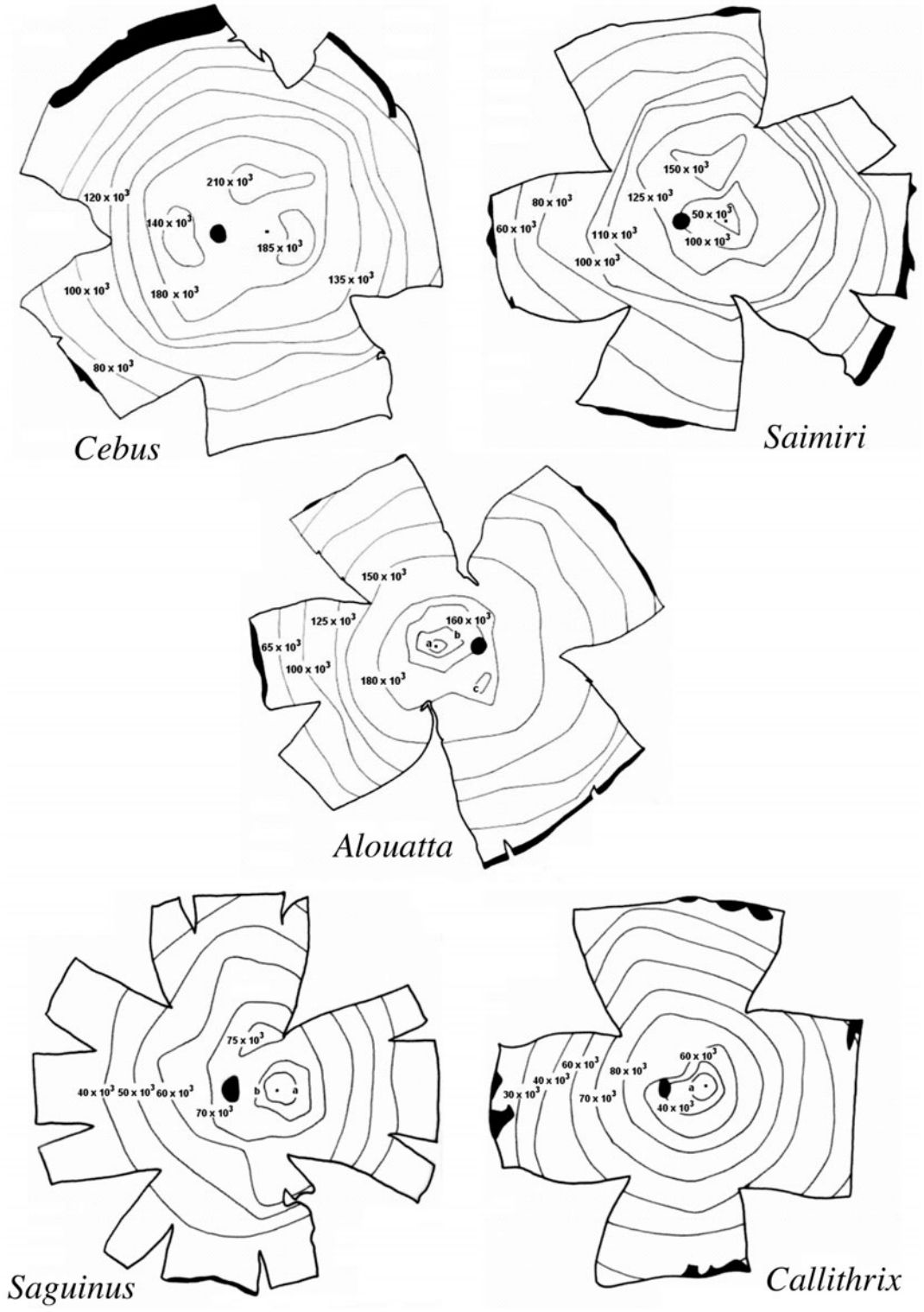

Fig. 4. Map of rod density in (**A**) *Cebus*, (**B**) *Saimiri*, (**C**) *Alouatta* Isodensity line a = 90 × 10^3, Isodensity line b = 125 × 10^3, Isodensity line c = 25 × 10^3, (**D**) *Saguinus* Isodensity line a = 30 × 10^3, Isodensity line b = 50 × 10^3, and (**E**) *Callithrix* Isodensity line a = 20 × 10^3. Variable scale as indicated by areal measurements listed in Fig. 3.

monkeys, with the notable exception of the human retina. There is little relationship of cone number to brain size (y = 0.0326x + 6.52; R^2= 0.173), and *Aotus* maintains its noticeable, but not large, reduction in cone number compared to the diurnal retinas. Optic nerve axon numbers scale significantly with brain size, but noisily (y = 0.1313x + 5.79; R^2 = 0.494), *Aotus* is more markedly reduced in numbers of retinal ganglion cells than cones. Rod number rises steeply with brain size over a full order of magnitude

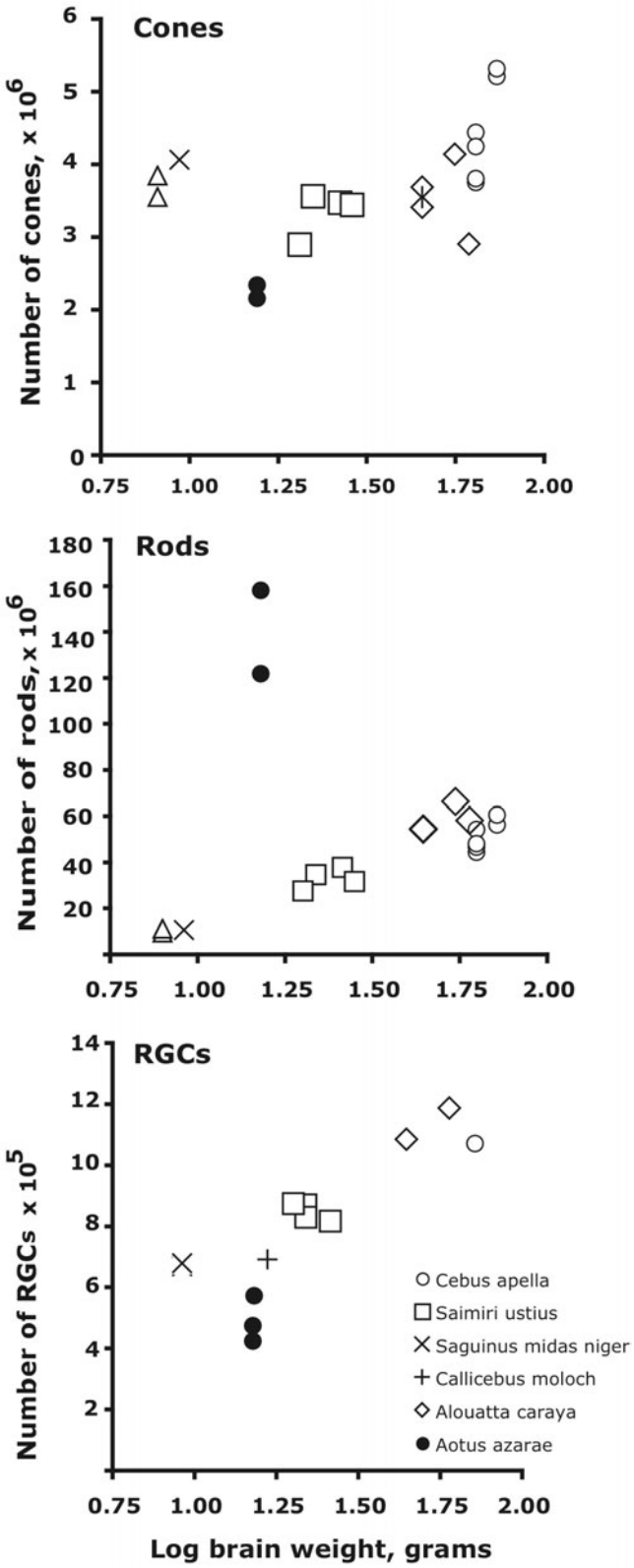

Fig. 5. Numbers of cones (**top**), rods (**middle**), and optic nerve axons (**bottom**) in individual New World monkeys indexed by log brain weight, semilog plot. Assessments of right and left sides of the same individual (Table 1) are plotted as separate points. ○, *Cebus apella;* □, *Saimiri ustius*; △, *Callithrix jacchus;* ×, *Saguinus midas niger*; ◇, *Allouatta caraya*; ●, *Aotus azarae*; +, *Callicebus moloch*.

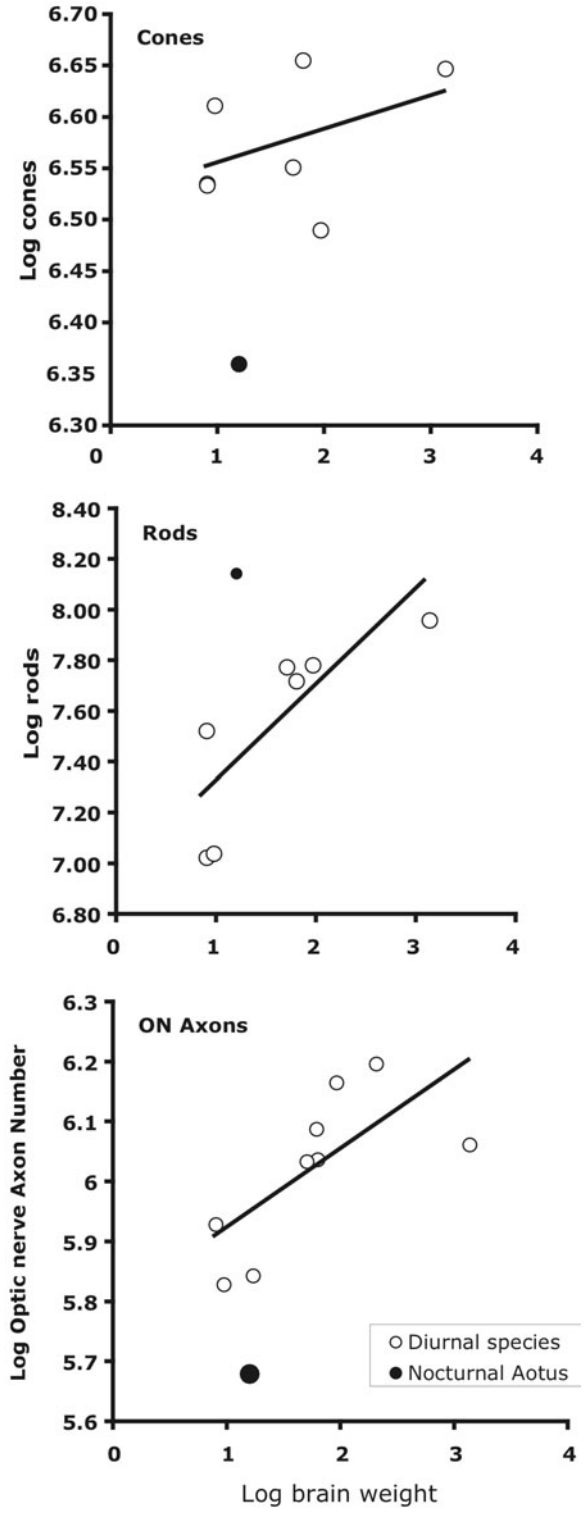

Fig. 6. Scaling of cones (**top**), rods (**middle**), and optic nerve axon numbers (**bottom**) as a function of brain weight by species listed in Table 2, log plot. This graph includes measurements in Old World monkeys and great apes as well as new World monkeys, and the sources for additional data are listed in Table 2. Each data point represents an average value for each species for cones, rods of optic nerve axon number. ○ diurnal primates; ●, *Aotus azarae*. Regression equations (diurnal primates only): cones: $y = 0.0326x + 6.52$; $R^2 = 0.173$. rods: $y = 0.3789 + 6.93$; $R^2 = 0.667$; optic nerve axons or retinal ganglion cells: $y = 0.1313x + 5.79$; $R^2 = 0.494$.

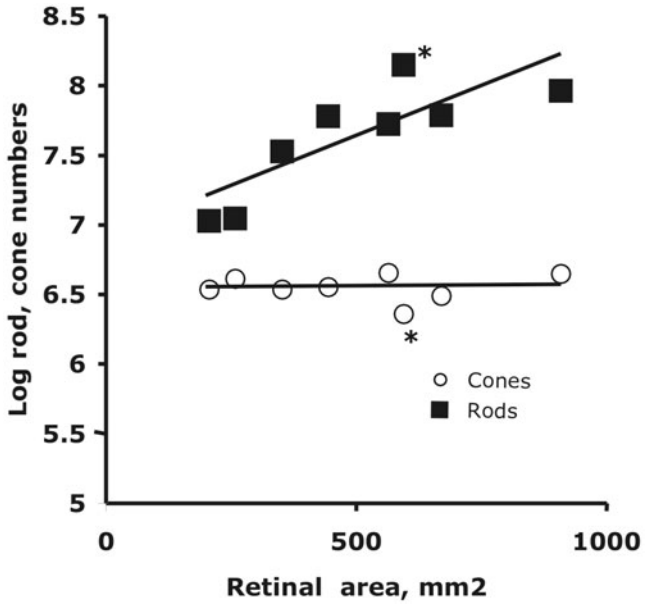

Fig. 7. Number of rods and cones as a function of retinal area, semilog plot. ■, rods; ○, cones. Species plotted are the New World Monkeys, plus *Macaca mulatta, Cercopithecus aethiops. Papio anubis* and *Homo sapien*s. Each data point represents an average value for each species for cones or rods. *Aotus azarae* (arrowed) has rod numbers above the regression line, and cones below. Regression equation (including all diurnal primates and *Aotus*): cones, $y = .0005x + 6.535$; $R^2 = 0.0045$; rods, $y = 0.0014x + 6.91$; $R^2 = 0.6776$.

($y = 0.3789 + 6.93$; $R^2 = 0.667$), and the excess rod number in *Aotus* is particularly striking. For each of rods, cones, and retinal ganglion cells, the human retina appears to have fewer cells than would be expected for its corresponding brain size.

The fundamental regularity underlying these data can be seen in Fig. 7, where rod and cone numbers are plotted against retina area rather than brain size. The relationship of cone number to retinal area is virtually flat ($y = .0005x + 6.535$; $R^2 = 0.0045$), while rod number scale significantly with retinal area ($y = 0.0014x + 6.91$; $R^2 = 0.678$). While *Aotus* (starred) continues to show an increment in rods and slight decrement in cones compared to the diurnal retinas, the human retina shows values of rod, and cone numbers appropriate to its area. If retinal area is regressed against brain size omitting humans, and the expected value for a human retina calculated, a retina of about 1100 mm^2 would be predicted, about 20% bigger that the 900 mm^2 observed value. Therefore, reduction of the size of the entire eye and retina in humans with respect to allometric prediction unites the observed decrement in the in human cones, rods, and retinal ganglion cell numbers.

Discussion

Quantification of retinal cell numbers

For this study, we have gathered information in the traditional manner for determination of cell numbers and isodensity contours (Stone, 1981). As both flat mounts of retinas for assessment of rods and cones, and a section of the optic nerve are two-dimensional surfaces, the only essential stereological requirement is to sample to avoid double counting, which was done by using excluded borders on the sampling rectangle. A sampling frequency was chosen that had been demonstrated to bring variability within acceptable limits in prior studies. The good allometric predictability of our observations (Figs. 5, 6, and 7) suggests that even with the limited sample sizes possible with primates, accurate assessments were made.

The overall pattern and its deviations

The diurnal primate retina shows a number of interesting regularities. First, the fovea remains the same *absolute* size in all primate retinas described to date. We have reported previously in these same animals that the size of the fovea, which can be measured in multiple ways including the inflection of the slope of maximum cone density, the region absent of overlying cell bodies, and from the rod-free area (except *Alouatta*), stays the same in absolute size, measuring about 0.5 mm in diameter (Franco et al., 2000). At the same time, the eye grows and the area of the retina expands by about a factor of four, necessarily reducing the angular subtense of the fovea from the marmoset to the human (Table 2). If for whatever reason the cellular mechanisms that produce the fovea are constrained to produce one of about 0.5 mm diameter at all retinal sizes, this may account for the failure to the human eye to scale with the allometry of smaller primates, as the fovea might become such a reduced visual angle as to compromise functionality.

Second, cones and rods, by virtue of their functional roles, should be expected to scale differently with respect to eye size, and the various sizes of primate eye duplicate a phenomenon observed in the constantly growing retinas of teleost fish (Hoke & Fernald, 1997). In order to maintain acuity, the number of cones need not increase with eye size, as the eye is flooded with photons, and any cone situated in a unit of visual angle, regardless of its metric size, will be able to register the presence of photons. For rods to maintain sensitivity, however, in situations of low photon capture, as the eye enlarges, the number of rods should increase so as to tile the retina and not miss capturing photons altogether. The differing tiling requirement for acuity versus sensitivity is of course a vertebrate-general problem, first described in fish (Muller, 1952; Johns, 1979). A particular developmental solution to the difficulty of maintaining rod sensitivity has been described in the cichlid fish *Haplochromus burtoni*, whose eye grows throughout life. The eye enlarges by addition of photoreceptors and all associated neural retina just at the retina periphery, resulting in a ring of cells associated with a unique retinal age. The one exception is for rods, where small rod-specific progenitor pools are located throughout the retina, interpolating new rods into the existing matrix (Hoke & Fernald, 1997).

Finally, in addition to the number of cells, the relationship of differential rod and cone neurogenesis to eye size produces characteristic differences in cell topography between small and large eyes. In the primate retina, as the eye becomes larger, cone gradients become steeper, including higher cone densities in the central retina, and lesser densities in the periphery. Rod gradients, due to the increased dose of rods in the larger retinas, do not change as much.

The principal deviations from the general retinal plan observed in these data are the following: the doubled rod density in the *Alouatta* retina, including a smaller rod-free zone, and diminished cone density peripherally. In *Aotus*, the owl monkey, cone and retinal ganglion cell numbers are reduced somewhat, a fovea is absent, and rod numbers are greatly increased; in addition, its retinal area is about 50% larger than would be predicted on the basis of comparable diurnal animals' brain sizes. In *Homo*, the numbers of retinal ganglion cells, rods, cones, and retinal area are all smaller than expected. We will argue that relatively simple

features and alterations of well-described developmental mechanisms that produce the retina can encompass the disproportionate scaling of rods and cones seen in eyes of graded sizes, and all the species-specific deviations noted.

Patterns of neurogenesis that may underlie rod and cone scaling

For explanatory convenience, primate retinal (and ocular) development can be conceived as the three processes of neurogenesis, foveal production, and retinal stretch (reviewed in Finlay et al., 2005). Neurogenesis sets up the basic matrix of cells in the retinal layers (Polley et al., 1989; LaVail et al., 1991). Next come compaction of cones in the fovea and displacement of overlying cell bodies (Packer et al., 1989; Hendrickson, 1994). Finally, concurrent in onset with foveal production but extending longer, the retina stretches in balloon fashion, which is most pronounced in the retinal periphery (for example, Robinson et al., 1989).

Here we consider primarily neurogenesis. In primates, as all mammals do, neurogenesis begins concurrently in the entire retina, first producing retinal ganglion cells and cones, then horizontal cells and amacrine cells, and finally rod bipolar cells, and rods (LaVail et al., 1991). Neurogenesis ceases first in the central retina, before many (or any) rods are produced, and extends much longer in the peripheral retina, when the cellular mechanisms specifying rod and bipolar production remain in force (Cepko et al., 1996). Extension of the period of neurogenesis, as is necessary to make a larger retina has likely direct consequences for the numbers and types of cells observed (Clancy et al., 1999). The longer time allows the cellular mechanisms specifying the cone-dense central retina to be separated both in space and in time from the rod-enriched peripheral retina, and along with retina stretch, produces the distinct gradients in the densities of various cell types seen in large retinas. Time compression conversely can account for the higher cone density in the periphery of the smaller retinas. Second, extension of the period of neurogenesis has disproportionate effects on late- and early-generated cells groups, which we have described in several other contexts (Finlay & Darlington, 1995; Finlay & Brodsky, 2006). In animals with extended periods of neurogenesis, late-generated cells receive a disproportionate boost in the number of their precursor cell pools, as those cell groups increase exponentially. Thus, the mammalian retina sites rod neurogenesis late in retinogenesis, where it will naturally scale at a rate higher than cones should protracted development produce a larger eye, presumably allowing graceful scaling of function in individual variability, and in consequence, in species variability.

Work is in progress to determine how the alteration of rod and cone cell complements in *Aotus* occurs in development. It is clear, however, that a hypothesis of retinal development informed by an evolutionary perspective is capable of generating a powerful explanatory framework for both retinal regularities and deviations.

Acknowledgments

Supported by CNPq numbers 910149/96-98 and NSF Int-9604599 to LCLS and BLF and NSF Grant IBN-0138113 to BLF. LCLS is supported by the FINEP research grant "Rede Instituto Brasileiro de Neurociência (IBN-Net)" number 01.06.0842-00. ECSF received a CAPES fellowship for graduate students. ESY and LCLS are CNPq research fellows. We thank Randy Snow, Barbara Clancy, Christine Collins, Shannon Caldwell, Melanie Studer and Jon Zurawski for their scientific and technical help with the electron microscopy.

References

Andrade da Costa, B.L.S. & Hokoç, J.L. (2000). Photoreceptor topography of the retina in the New World monkey *Cebus apella*. *Vision Research* **40**, 2395–2409.

Cepko, C.L., Austin, C.P., Yang, X.J. & Alexiades, M. (1996). Cell fate determination in the vertebrate retina. *Proceedings of the National Academy of Sciences USA* **93**, 589–595.

Clancy, B., Darlington, R.B. & Finlay, B.L. (1999). The course of human events: Predicting the timing of primate neural development. *Developmental Science* **3**, 57–66.

Cull, G.B., Cioffi, G.A., Dong, J., Homer, L. & Wang, L. (2003). Estimating normal optic nerve axon numbers in non-human primate eyes. *Journal of Glaucoma* **12**, 301–306.

Curcio, C.A., Packer, O. & Kalina, R.E. (1987). A whole mount method for sequential analysis of photoreceptor and ganglion cell topography in a single retina. *Vision Research* **27**, 9–15.

Curcio, C.A., Sloan, K.R., Kalina, R.E. & Hendrickson, A.E. (1990). Human photoreceptor topography. *Journal of Comparative Neurology* **292**, 497–523.

Finlay, B.L. & Brodsky, P.B. (2006). Cortical evolution as the expression of a program for disproportionate growth and the proliferation of areas. In *Evolution of Nervous Systems, Mammals*, vol. 3. ed. Kaas, J.H. & Krubitzer, L.A., pp. 73–96. Oxford: Academic Press.

Finlay, B.L. & Darlington, R.B. (1995). Linked regularities in the development and evolution of mammalian brains. *Science* **268**, 1578–1584.

Finlay, B.L., Dyer, M.A., da Silva Filho, M., Muniz, J.A.P.C. & Silveira, L.C.L. (2007). Developmental programs coordinating size and niche variations in the primate eye and retina. In *Abstracts Book of the 19th Symposium of the International Colour Vision Society (ICVS)*, ed. Silveira, L.C.L., Ventura, D.F. & Lee, B.B., pp. 67–68. Belém, Brazil: EDUFPA.

Finlay, B.L., Silveira, L.C.L. & Reichenbach, A. (2005). Comparative aspects of visual system development. In *The Structure, Function and Evolution of the Primate Visual System*. ed. Kremers, J., pp. 37–72. New York: John Wiley & Sons.

Fischer, Q.S. & Kirby, M.A. (1991). Number and distribution of retinal ganglion cells in anubis baboons (*Papio anubis*). *Brain, Behavior and Evolution* **37**, 189–204.

Fleagle, J.G. (1988). *Primate Evolution and Adaptation*. New York: Academic Press.

Franco, E.C.S., Finlay, B.L., Silveira, L.C.L., Yamada, E.S. & Crowley, J.C. (2000). Conservation of absolute foveal area in new world monkeys—A constraint on eye size and conformation. *Brain Behavior and Evolution* **56**, 276–286.

Franco, E.C.S., Yamada, E.S., Silveira, L.C.L. & Finlay, B.L. (2007). Distribution and total number of the photoreceptors in callitrichin primates: *Callithrix jacchus jacchus* and *Saguinus midas niger*. In *Abstracts Book of the 19th Symposium of the International Colour Vision Society (ICVS)*, ed. Silveira, L.C.L., Ventura, D.F. & Lee, B.B., pp. 177–178. Belém, Brazil: EDUFPA.

Gerhart, J. & Kirschner, M. (1997). *Cells, Embryos and Evolution*. Malden, MA: Blackwell Science.

Heesy, C.P. & Ross, C.F. (2001). Evolution of activity patterns and chromatic vision in primates: morphometrics, genetics and cladistics. *Journal of Human Evolution* **40**, 111–149.

Hendrickson, A.E. (1994). Primate foveal development: A microcosm of current questions in neurobiology. *Investigative Ophthalmology and Visual Science* **35**, 3129–3133.

Herbin, M., Boire, D. & Ptito, M. (1997). Size and distribution of retinal ganglion cells in the St. Kitts green monkey (*Cercopithecus aethiops sabeus*). *Journal of Comparative Neurology* **383**, 459–472.

Hoke, K.L. & Fernald, R.D. (1997). Rod photoreceptor neurogenesis. *Progress in Retinal and Eye Research* **16**, 31–49.

Jacobs, G.H. (1998). Photopigments and seeing—Lessons from natural experiments—The Proctor Lecture. *Investigative Ophthalmology and Visual Science* **39**, 2205–2216.

Jacobs, G.H., Neitz, M. & Neitz, J. (1996). Mutations in S-cone pigment genes and absence of color vision in two species of nocturnal primate. *Proceedings of the Royal Society of London B* **263**, 705–710.

Johns, P.R. (1979). Growth and neurogenesis in adult goldfish retina. In *Developmental Neurobiology of Vision*, vol. 27, ed. Freeman, R.D., pp. 345–357. New York: Plenum.

Jonas, J.B., Schmidt, A.M., Mullerbergh, J.A., Schlotzerschrehardt, U.M. & Nauman, G.O.H. (1992). Human optic nerve fiber

count and optic disc size. *Investigative Ophthalmology and Visual Science* **33**, 2012–2018.

Kainz, P.M., Neitz, J. & Neitz, M. (1998). Recent evolution of uniform trichromacy in a New World monkey. *Vision Research* **38**, 3315–3320.

LaVail, M.M., Rapaport, D.H. & Rakic, P. (1991). Cytogenesis in the monkey retina. *Journal of Comparative Neurology* **309**, 86–114.

Muller, H. (1952). Bau und Wachstum der Nezhaut des Guppy (*Lebistes reticulatus*). *Zoologisches Jahrbuch. Abteilung Allg. Zool. Physiol*. **63**, 275–324.

Nagamachi, C.Y., Pieczarka, J.C., Muniz, J., Barros, R.M.S. & Mattevi, M.S. (1999). Proposed chromosomal phylogeny for the South American primates of the Callitrichidae family (Platyrrhini). *American Journal of Primatology* **49**, 133–152.

Naito, J. (1996). Morphological and quantitative analysis of the fascicular pattern of monkey optic nerve. *Cell and Tissue Research* **283**, 255–261.

Ogden, T.E. (1975). The receptor mosaic of *Aotes trivirgatus*: distribution of rods and cones. *Journal of Comparative Neurology* **163**, 193–202.

Packer, O., Hendrickson, A.E., Curcio, C.A. (1989). Developmental redistribution of photoreceptors across the *Macaca nemestrina* (pigtail macaque). *Journal of Comparative Neurology* **288**, 165–183.

Perry, V.H. & Cowey, A. (1985). The ganglion cell and cone distributions in the monkey's retina: Implications for central magnification factors. *Vision Res*. **25**, 1795–1810.

Polley, E.H., Zimmerman, R.P. & Fortney, R.L. (1989). Neurogenesis and maturation of cell morphology in the development of the mammalian retina. In *Development of the Vertebrate Retina*. ed. Finlay, B.L. & Sengelaub, D.R., pp. 3–29. New York: Plenum.

Rakic, P. (1983). Regulation of axon number in primate optic nerve by prenatal binocular competition. *Nature* **305**, 135–137.

Reese, B.E. & Ho, K.-Y. (1988). Axon diameter distributions across monkey optic nerve. *Neuroscience* **27**, 205–214.

Robinson, S.R., Dreher, B. & McCall, M.J. (1989). Nonuniform retinal expansion during the formation of the rabbit's visual streak: Implications for the ontogeny of mammalian retinal topography. *Visual Neuroscience* **2**, 201–219.

Ross, C.F. (2000). Into the light: The origin of Anthropoidea. *Annual Review of Anthropology* **29**, 147–194.

Schneider, H., Sampaio, I., Harada, M.L., Barroso, C.M.L., Schneider, M.P.C., Czelusniak, J. & Goodman, M. (1996). Molecular phylogeny of the New World Monkeys (Platyrrhini, Primates) based on two unlinked nuclear genes: IRBP intron 1 and e-globin sequences. *American Journal of Physical Anthropoogy* **100**, 153–179.

Schneider, H. (2000). The current status of the New World monkey phylogeny. *Anais da Academia Brasileira de Ciências* **72**, 165–172.

Silveira, L.C.L., Pincanco-Diniz, C.W., Sampaio, L.F.S. & Oswaldo-Cruz, E. (1989). Retinal ganglion cell distribution in the cebus monkey: A comparison with the cortical magnification factors. *Vision Research* **29**, 1471–1483.

Silveira, L.C.L., Perry, V.H. & Yamada, E.S. (1993). The retinal ganglion cell distribution and the representation of the visual field in Area 17 of the owl monkey, *Aotus trivirgatus*. *Visual Neuroscience* **10**, 887–897.

Silveira, L.C.L., Yamada, E.S., Franco, E.C.S. & Finlay, B.L. (2001). The specialization of the owl monkey retina for night vision. *Colour Research and Application* **26**, S118–S122.

Silveira, L.C.L., Zurawski, J.D., Parsons, M.P. & Finlay, B.L. (2004). Unusual retinal organization in the howler monkey. *Alouatta caraya*. *Investigative Ophthalmology and Visual Science* **45**, E-Abstract 44.

Snow, R.L., Nelson, A., Driscoll, L.L., Hartman, K.L., Silveira, L.C.L. & Finlay, B.L. (1997). Scaling of the visual system, photoreceptors to extrastriate cortex, emphasizing primates. *Society for Neuroscience Abstracts* **23**, 1308.

Stephan, H., Frahm, H. & Baron, G. . (1981). New and revised data on volumes of brain structures in insectivores and primates. *Folia Primatologica* **35**, 1–29.

Stone, J. (1981). The whole mount handbook. A guide to the preparation and analysis of retinal whole mounts. Sidney: Maitland Publ PTY Ltd.

Troilo, D., Howland, H.C., Judge, S.J. (1993). Visual optics and retinal cone topography in the common marmoset (*Callithrix jacchus*). *Vision Research* **33**, 1301–1310.

Wikler, K.C. & Rakic, P. (1990). Distribution of photoreceptor subtypes in the retina of diurnal and nocturnal primates. *The Journal of Neuroscience* **10**, 3390–3401.

Wikler, K.C., Williams, R.C., Rakic, P. (1990). The photoreceptor mosaic: Number and distribution of rods and cones in the *Rhesus* monkey retina. *Journal of Comparative Neurology* **297**, 499–508.

Wilder, H.D., Grünert, U., Lee, B.B., Martin, P.R. (1996). Topography of ganglion cells and photoreceptors in the retina of a New World monkey: The marmoset *Callithrix jacchus*. *Visual Neuroscience* **13**, 335–352.